9th AIAA/ISSMO Symposium on Multidisciplinary Analysis and Optimization
4-6 September 2002, Atlanta, Georgia

AIAA 2002-5541

SHAPE OPTIMIZATION OF TWO-DIMENSIONAL AUTOMOTIVE COMPONENTS USING A MESHFREE METHOD

Mark E. Botkin*, Hui-Ping Wang†
GM R&D Center
Warren, MI 48090-9055

Nam Ho Kim
Department of Mechanical Engineering
University of Florida, PO Box 116300
Gainesville, FL 32611-6300

Kyung K. Choi
Center for Computer Aided Design, College of Engineering
The University of Iowa
Iowa City, IA 52242

ABSTRACT

The Reproducing Kernel Particle Method (RKPM) is one of several so-called meshfree methods of structural analysis and has been applied in this paper to the gradient-based shape optimization of two-dimensional automotive components. As indicated by the term meshfree, no mesh is required, but rather a field of points, or particles, are distributed within the domain of the problem. Three standard linear examples are chosen to allow a comprehensive comparison between the optimization with the RKPM and the state-of-art optimization tool in Unigraphics Version 18 (UG V18). The results show that the optimization analysis with the RKPM is able to accommodate very large shape changes required in the optimization process without doing particle re-adaptation, and provides accurate solutions of the objective and constraint functions and their gradients, therefore facilitates a fast convergence of the gradient-based optimization algorithm.

INTRODUCTION

Loss of solution accuracy due to the excessive mesh distortion that occurs during large shape changes constitutes one of the major computational challenges in structural shape optimization with the finite element method (FEM). A common and direct approach to avoid the mesh distortion is to perform mesh adaptations or re-meshing during the optimization process (see Bennett and Botkin[1], and Yao and Choi[2]). However, this approach is so expensive that it becomes unaffordable for large automotive models.

In recent years, meshfree methods have been proposed for structural analyses to overcome the aforementioned mesh-related difficulties. Typical meshfree methods are moving least squares method in Lancaster and Slakauskas[3], smooth particle hydrodynamics method in Randles and Libersky[4], diffuse element method in Nayroles et al.[5], element free Galerkin method in Belytschko et al.[6], reproducing kernel particle method (RKPM) in Liu et al.[7] and Chen et al.[8], partition of unity method in Melenk and Babuska[9], and hp–cloud method in Duarte and Oden[10]. The common characteristic of the meshfree methods is that their shape/approximation functions are constructed entirely based on a set of discrete points/particles with no requirement of particular topological connection among the points. Mesh distortion difficulties are naturally resolved in the meshfree methods, since the connectivity among the points is only used for the purpose of the domain integration in the solutions of partial differential equations (PDEs) in a galerkin scheme, and is independent of the meshfree approximation. Substantial evidence shows that the meshfree methods have strong tolerance of irregular nodal discretization without loss of solution accuracy, not to mention their convenience in achieving h & p-adaptivity.

Meshfree-based design sensitivity analysis (DSA) research was started in 1998 by Grindeanu et al.[11] for hyper-elastic problems and later on continued by Kim et al.[12-14] for the elastic-plastic and contact problems using the RKPM. The advantages of the RKPM in the DSA research have been shown in their papers in terms of accurate sensitivity computation and strong capabilities in handling large shape changes.

The purpose of this paper is to employ the RKPM-

---

* Principal Research Engineer, Member AIAA
† Senior Research Engineer

based DSA for the gradient-based shape optimization analysis of automotive components, and to allow the benchmark of the meshfree-based optimization process with the state-of-art shape optimization in UG V18. In the following sections, the reproducing kernel particle method for structural analysis is reviewed first. Then the meshfree design sensitivity formulation is introduced. Numerical examples are presented next. Conclusions and summaries are given at the end.

REPRODUCING KERNEL PARTICLE METHOD

The reproducing kernel particle approximation was proposed by Liu et al.[7] and developed for the solutions of structural problems by Liu et al.[7] and Chen et al.[8].

Reproducing Kernel Particle Approximation

Assume that the given domain $\Omega \in R^2$ is discretized by a set of particles $[\boldsymbol{x}^1,\ldots, \boldsymbol{x}^I,\ldots, \boldsymbol{x}^{NP}]$, where $\boldsymbol{x}^I=[x^I, y^I]^T=[x_1^I, x_2^I]^T$ is the location of particle I, and NP is the total number of particles, the discrete reproducing kernel particle approximation of the function $f(\boldsymbol{x})$ is

$$f^R(\boldsymbol{x}) = \sum_{I=1}^{NP} C(\boldsymbol{x};\boldsymbol{x}^I-\boldsymbol{x})\phi_a(\boldsymbol{x}^I-\boldsymbol{x})\, f^I \qquad (1)$$

where $f^R(\boldsymbol{x})$ is the reproduced (approximated) function of $f(\boldsymbol{x})$, ϕ_a is the kernel function which defines the smoothness of the approximation with a compact support measured by "a". A common form of the one-dimensional kernel functions utilizes a cubic spline function, which is

$$\phi_a(s) = \frac{1}{6a}\begin{cases} (3s^3-6s^2+4), & 0\le s\le 1 \\ -(s-2)^3, & 1\le s\le 2 \\ 0, & \text{otherwise} \end{cases};$$

$$s = \left|(x^I - x)/a\right| \qquad (2)$$

For particle $\boldsymbol{x}^I$ with a support size $\boldsymbol{a}=[a_1, a_2]$, its kernel function is defined as $\phi_{\mathbf{a}}(\mathbf{x}^I-\mathbf{x}) = \phi_{a_1}((x_1^I-x_1)/a_1)\phi_{a_2}((x_2^I-x_2)/a_2)$.

$C(\boldsymbol{x}; \boldsymbol{x}^I-\boldsymbol{x})$ in Equation (1) is a correction function that is a linear combination of monomial basis functions:

$$C(\boldsymbol{x};\boldsymbol{x}^I-\boldsymbol{x}) = \sum_{i+j=0}^{n} (x_1^I-x_1)^i (x_2^I-x_2)^j q_{ij}(\boldsymbol{x}) \equiv \boldsymbol{q}(\boldsymbol{x})^T \boldsymbol{H}(\boldsymbol{x}^I-\boldsymbol{x}) \qquad (3)$$

$$\boldsymbol{H}(\boldsymbol{x}^I-\boldsymbol{x}) = \left[1, x_1^I-x_1, x_2^I-x_2, (x_1^I-x_1)^2, \cdots, (x_2^I-x_2)^n\right]^T \qquad (4)$$

where $\boldsymbol{H}(\boldsymbol{x}^I-\boldsymbol{x})$ is the vector of monomial basis functions. The coefficient vector $\boldsymbol{q}(\boldsymbol{x})$ facilitates the discrete reproducing conditions, which are,

$$\sum_{I=1}^{NP} C(\boldsymbol{x};\boldsymbol{x}^I-\boldsymbol{x})\phi_a(\boldsymbol{x}^I-\boldsymbol{x}) x_{1I}^i x_{2I}^j = \sum_{I=1}^{NP} \boldsymbol{q}(\boldsymbol{x})^T \boldsymbol{H}(\boldsymbol{x}^I-\boldsymbol{x})\phi_a(\boldsymbol{x}^I-\boldsymbol{x}) x_{1I}^i x_{2I}^j = x_1^i x_2^j,\ i+j=0,\cdots,n \qquad (5)$$

Equation (5) is equivalent to

$$\sum_{I=1}^{NP} \boldsymbol{q}(\boldsymbol{x})^T \boldsymbol{H}(\boldsymbol{x}^I-\boldsymbol{x})\phi_a(\boldsymbol{x}^I-\boldsymbol{x})(x_{1I}-x_1)^i (x_{2I}-x_2)^j = \delta_{i0}\delta_{j0},\ i+j=0,\cdots,n \qquad (6)$$

By solving $\boldsymbol{q}(\boldsymbol{x})$ from the reproducing equation (6), the correction function can be determined as

$$C(\boldsymbol{x};\boldsymbol{x}^I-\boldsymbol{x}) = \boldsymbol{H}^T(\boldsymbol{0})\boldsymbol{M}^{-1}(\boldsymbol{x})\boldsymbol{H}(\boldsymbol{x}^I-\boldsymbol{x}) \qquad (7)$$

where $\boldsymbol{M}(\boldsymbol{x})$ is the moment matrix, defined as

$$\boldsymbol{M}(\boldsymbol{x}) = \sum_{I=1}^{NP} \phi_a(\boldsymbol{x}^I-\boldsymbol{x})\boldsymbol{H}(\boldsymbol{x}^I-\boldsymbol{x})\boldsymbol{H}^T(\boldsymbol{x}^I-\boldsymbol{x}) \qquad (8)$$

Substituting the correction function in Equation (7) into Equation (1) leads to the reproducing approximation

$$f^R(\boldsymbol{x}) = \sum_{I=1}^{NP} \boldsymbol{H}^T(\boldsymbol{0})\boldsymbol{M}^{-1}(\boldsymbol{x})\boldsymbol{H}(\boldsymbol{x}^I-\boldsymbol{x})\phi_a(\boldsymbol{x}^I-\boldsymbol{x})\, f^I \equiv \sum_{I=1}^{NP} \Phi^I(\boldsymbol{x})\, f^I \qquad (9)$$

where $\Phi^I(\boldsymbol{x})$ is called the *meshfree shape function* of particle I:

$$\Phi^I(\boldsymbol{x}) = \boldsymbol{H}^T(\boldsymbol{0})\boldsymbol{M}^{-1}(\boldsymbol{x})\boldsymbol{H}(\boldsymbol{x}^I-\boldsymbol{x})\phi_a(\boldsymbol{x}^I-\boldsymbol{x}), \qquad (10)$$

and its partial derivatives are calculated as

$$\Phi^I_{,k}(\boldsymbol{x}) = \boldsymbol{H}^T(\boldsymbol{0})\boldsymbol{M}^{-1}_{,k}(\boldsymbol{x})\boldsymbol{H}(\boldsymbol{x}^I-\boldsymbol{x})\phi_a(\boldsymbol{x}^I-\boldsymbol{x}) + \boldsymbol{H}^T(\boldsymbol{0})\boldsymbol{M}^{-1}(\boldsymbol{x})\boldsymbol{H}_{,k}(\boldsymbol{x}^I-\boldsymbol{x})\phi_a(\boldsymbol{x}^I-\boldsymbol{x}) + \boldsymbol{H}^T(\boldsymbol{0})\boldsymbol{M}^{-1}(\boldsymbol{x})\boldsymbol{H}(\boldsymbol{x}^I-\boldsymbol{x})\phi_{a,k}(\boldsymbol{x}^I-\boldsymbol{x}) \qquad (11)$$

where $(\cdot)_{,k}$ denotes the spatial derivative $\partial(\cdot)/\partial x_k$, k=1,2.

Differing from the finite element shape functions, the meshfree shape functions do not have Kronecker delta properties, i.e., $\Phi^I(\boldsymbol{x}^J) \neq \delta_{IJ}$. The coefficient f^I is the nodal value of the function $f(\boldsymbol{x})$ at particle I in the case that $f(\boldsymbol{x})$ is a monomial function. When the approximated functions are non-monomial functions, the coefficients are in general not the nodal values. Therefore, when the reproducing kernel particle approximation is applied to a displacement function $\boldsymbol{z}(\boldsymbol{x})$, it is rewritten as

$$\begin{aligned} \boldsymbol{z}^R(\boldsymbol{x}) &= \sum_{I=1}^{NP} \boldsymbol{H}^T(\boldsymbol{0})\boldsymbol{M}^{-1}(\boldsymbol{x})\boldsymbol{H}(\boldsymbol{x}^I-\boldsymbol{x})\phi_a(\boldsymbol{x}^I-\boldsymbol{x})\boldsymbol{d}^I \\ &\equiv \sum_{I=1}^{NP} \Phi^I(\boldsymbol{x})\boldsymbol{d}^I \end{aligned} \tag{12}$$

where the coefficient $\boldsymbol{d}^I$ is called the *generalized displacement* of particle *I*, which is not the nodal value of $\boldsymbol{z}(\boldsymbol{x}^I)$. Because of this absence of Kronecker Delta properties, special techniques are required to impose the essential boundary conditions in the solutions of boundary value problems. In this paper, the mixed transformation method presented in Chen and Wang[15] is employed for this purpose.

Meshfree Small Strain Elastic Formulation

The variational form of the continuum equilibrium equation of small strain elastic structural problems is

$$\begin{aligned} a_\Omega(\boldsymbol{z},\bar{\boldsymbol{z}}) &\equiv \iint_\Omega \sigma_{ij}\varepsilon_{ij}(\bar{\boldsymbol{z}})\,d\Omega \\ &= \iint_\Omega \bar{z}_i b_i\,d\Omega \equiv \ell_\Omega(\bar{\boldsymbol{z}}), \qquad \forall \bar{\boldsymbol{z}} \in Z \end{aligned} \tag{13}$$

where σ_{ij} and ε_{ij} are the stress and strain tensors, respectively; $\boldsymbol{z}$, $\bar{\boldsymbol{z}}$ and $\boldsymbol{b}$ are the displacement vector, the displacement variation and the body force vector, respectively; *Z* is the space of kinematically admissible displacements that satisfy homogeneous essential boundary conditions; Ω is the domain of interest; $a_\Omega(\boldsymbol{z},\bar{\boldsymbol{z}})$, $\ell_\Omega(\bar{\boldsymbol{z}})$ and "–" denote the structural energy, the external load and the variation of a quantity, respectively. For the sake of simplicity, traction boundary conditions are not considered here. The constitutive relation of linear elastic materials is given as

$$\sigma_{ij}(\boldsymbol{z}) = c_{ijkl}\varepsilon_{kl}(\boldsymbol{z}) \tag{14}$$

where c_{ijkl} is the 4th–order stiffness tensor.

Applying the meshfree approximation in Equation (12) to the displacement and its variation in Equation (13), and employing the mixed transformation method for the imposition of essential boundary conditions, one can obtain a discrete system of equations as

$$\boldsymbol{K}^*\boldsymbol{d} = \boldsymbol{f}^* \tag{15}$$

where

$$\boldsymbol{K}^* = \boldsymbol{\Lambda}^{*-\mathrm{T}}\boldsymbol{K} \tag{16}$$

$$\boldsymbol{f}^* = \boldsymbol{\Lambda}^{*-\mathrm{T}}\boldsymbol{f} \tag{17}$$

$$\boldsymbol{K}_{\mathrm{IJ}} = \int_\Omega \boldsymbol{B}_{\mathrm{I}}^{\mathrm{T}}\boldsymbol{C}\boldsymbol{B}_{\mathrm{J}}\,\mathrm{d}\Omega \tag{18}$$

$$\boldsymbol{f}_{\mathrm{I}} = \int_\Omega \Phi^{\mathrm{I}}\boldsymbol{b}\,\mathrm{d}\Omega \tag{19}$$

where $\boldsymbol{C}$ is the material matrix corresponding to c_{ijkl}, $\boldsymbol{d}=[\boldsymbol{d}^1, \boldsymbol{d}^2,\ldots,\boldsymbol{d}^{NP}]^T$ the generalized displacement vector, $\boldsymbol{K}$ the generalized stiffness matrix, and $\boldsymbol{f}$ the external force vector. The definition of the mixed transformation matrix $\boldsymbol{\Lambda}^*$ can be found in Chen and Wang[15]. For two-dimensional problems, $\boldsymbol{B}$ matrix is defined by

$$\boldsymbol{B}_I = \begin{bmatrix} \Phi^I_{,1} & \Phi^I_{,2} & 0 \\ 0 & \Phi^I_{,1} & \Phi^I_{,2} \end{bmatrix}^T. \tag{20}$$

The integration over the domain Ω is achieved by partitioning the structural domain into non-overlapping integration zones $\Omega = \Omega^1 \cup \cdots \cup \Omega^N$ and employing the standard Gauss integration as shown in Figure 1. The solution of Equation (15) leads to the determination of the displacements $\boldsymbol{z}$ by $\boldsymbol{z}^R(\boldsymbol{x}) = \sum_{I=1}^{NP} \Phi^I(\boldsymbol{x})\boldsymbol{d}^I$.

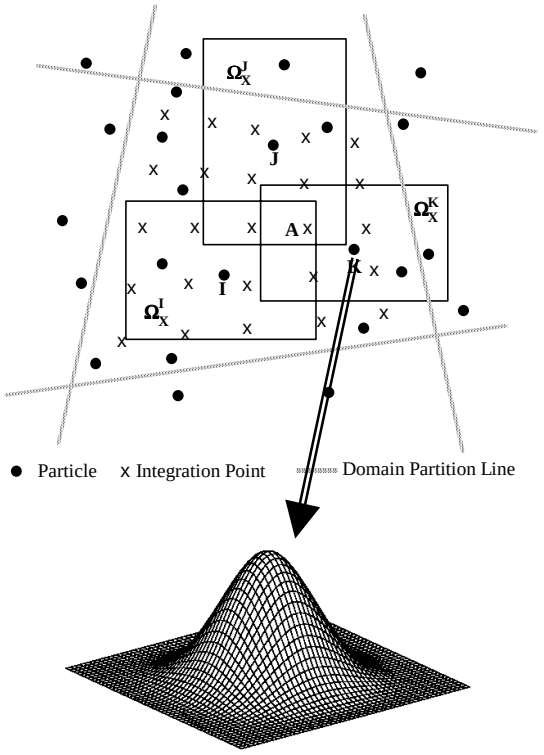

Figure 1. Domain Discretization and Meshfree Shape Function

SHAPE DESIGN SENSITIVITY FORMULATION

Assume that the initial structural domain Ω with boundary Γ is changed into a new domain Ω_τ with boundary Γ_τ. The material point at the new design is related to the initial design by $\boldsymbol{x}_\tau = \boldsymbol{x} + \tau\boldsymbol{V}(\boldsymbol{x})$, where $\boldsymbol{V}(\boldsymbol{x})$ defines the design changing direction and the

parameter τ controls the amount of shape change. The solution $\boldsymbol{z}_\tau(\boldsymbol{x}_\tau)$ of structural problems is assumed a differentiable function with respect to shape design. The material derivative of $\boldsymbol{z}_\tau(\boldsymbol{x}_\tau)$ at $\boldsymbol{x}_\tau \in \Omega_\tau$ is defined as

$$\dot{\boldsymbol{z}} = \lim_{\tau \to 0} \frac{\boldsymbol{z}_\tau\left(\boldsymbol{x} + \tau \boldsymbol{V}(\boldsymbol{x})\right) - \boldsymbol{z}(\boldsymbol{x})}{\tau} \tag{21}$$

In this paper, it is assumed that the space Z of kinematically admissible displacements is independent of shape design, i.e., $\dot{\bar{\boldsymbol{z}}} = 0$. The design sensitivity equation is obtained by taking the material derivative of the continuum equilibrium equation in Equation (13) as

$$a_\Omega(\dot{\boldsymbol{z}}, \bar{\boldsymbol{z}}) = \ell'_V(\bar{\boldsymbol{z}}) - a'_V(\boldsymbol{z}, \bar{\boldsymbol{z}}), \forall \bar{\boldsymbol{z}} \in Z \tag{22}$$

where

$$\begin{aligned} a'_V(\boldsymbol{z}, \bar{\boldsymbol{z}}) = & \iint_\Omega [\varepsilon_{ij}^V(\bar{\boldsymbol{z}}) \sigma_{ij}(\boldsymbol{z}) + \varepsilon_{ij}(\bar{\boldsymbol{z}}) c_{ijkl} \varepsilon_{kl}^V(\boldsymbol{z})] d\Omega \\ & + \iint_\Omega [\varepsilon_{ij}(\bar{\boldsymbol{z}}) \sigma_{ij}(\boldsymbol{z}) div\mathbf{V}] d\Omega \end{aligned} \tag{23}$$

$$\ell'_V(\bar{\boldsymbol{z}}) = \iint_\Omega [\bar{\boldsymbol{z}}^T (\nabla \boldsymbol{b} \boldsymbol{V}) + \bar{\boldsymbol{z}}^T \boldsymbol{b}\, div \boldsymbol{V}] d\Omega \tag{24}$$

$$\varepsilon_{ij}^V(\boldsymbol{z}) = -\frac{1}{2}\left(\frac{\partial z_i}{\partial x_k}\frac{\partial V_k}{\partial x_j} + \frac{\partial z_j}{\partial x_k}\frac{\partial V_k}{\partial x_i} \right) \tag{25}$$

The term on the left side of Equation (22) represents an implicit dependence of the structural energy on the design through the state variable, the first term on the right side is the external fictitious load form, and the second term is the structural fictitious load which denotes an explicit dependence of the structural energy on the design velocity $\boldsymbol{V}(\boldsymbol{x})$.

Note that by substituting $\dot{\boldsymbol{z}}$ into $\boldsymbol{z}$, the left of the design sensitivity equation (22) takes the same form as that of the response analysis in Equation (13). Thus, the same stiffness matrix can be used for DSA as the one for response analysis, but with a different right side for the fictitious load.

The meshfree approximation of $\dot{\boldsymbol{z}}$ can be obtained by the direct differentiation of the approximation of $\boldsymbol{z}$ in Equation (12) as

$$\dot{\boldsymbol{z}}^R = \sum_{I=1}^{NP} (\Phi^I \dot{\boldsymbol{d}}^I + \dot{\Phi}^I \boldsymbol{d}^I) \tag{26}$$

The first term of Equation (26) constitutes the main unknown $\dot{\boldsymbol{d}}$ of the design sensitivity equation in meshfree approximation, while the second term represents the dependence of the shape function on design, which is explicit in $\boldsymbol{V}(\boldsymbol{x})$. Note that this dependence is different from the FEM in which the shape function is independent of the design, i.e. $\dot{\Phi}^I = 0$. $\dot{\Phi}^I(\boldsymbol{x})$ in RKPM can be calculated as

$$\begin{aligned} \dot{\Phi}^{\mathrm{I}}(\boldsymbol{x}) = & \boldsymbol{H}^{\mathrm{T}}(\boldsymbol{0}) \dot{\boldsymbol{M}}^{-1}(\boldsymbol{x}) \boldsymbol{H}(\boldsymbol{x}^{\mathrm{I}} - \boldsymbol{x}) \phi_{\mathrm{a}}(\boldsymbol{x}^{\mathrm{I}} - \boldsymbol{x}) \\ & + \boldsymbol{H}^{\mathrm{T}}(\boldsymbol{0}) \boldsymbol{M}^{-1}(\boldsymbol{x}) \dot{\boldsymbol{H}}(\boldsymbol{x}^{\mathrm{I}} - \boldsymbol{x}) \phi_{\mathrm{a}}(\boldsymbol{x}^{\mathrm{I}} - \boldsymbol{x}) \\ & + \boldsymbol{H}^{\mathrm{T}}(\boldsymbol{0}) \boldsymbol{M}^{-1}(\boldsymbol{x}) \boldsymbol{H}(\boldsymbol{x}^{\mathrm{I}} - \boldsymbol{x}) \dot{\phi}_{\mathrm{a}}(\boldsymbol{x}^{\mathrm{I}} - \boldsymbol{x}) \end{aligned} \tag{27}$$

where

$$\dot{\phi}_a(s) = \frac{V^I - V}{2a^2} \begin{cases} (3s^2 - 4s), & 0 \le s \le 1 \\ -(s-2)^2, & 1 \le s \le 2 \\ 0, & \text{otherwise} \end{cases} \tag{28}$$

$$\begin{aligned} & \dot{\boldsymbol{H}}(\boldsymbol{x}^I - \boldsymbol{x}) \\ & = [0, V_1^I - V_1, V_2^I - V_2, 2(x_1^I - x_1)(V_1^I - V_1), \\ & \qquad \cdots, n(x_2^I - x_2)^{n-1}(V_2^I - V_2)]^T \end{aligned} \tag{29}$$

$$\begin{aligned} & \dot{\boldsymbol{M}}^{-1} \\ & = -\boldsymbol{M}^{-1}[\sum_{I=1}^{NP} (\dot{\phi}_a \boldsymbol{H}\boldsymbol{H}^T + \phi_a \dot{\boldsymbol{H}}\boldsymbol{H}^T + \phi_a \boldsymbol{H}\dot{\boldsymbol{H}}^T)]\boldsymbol{M}^{-1} \end{aligned} \tag{30}$$

and $\boldsymbol{V}^I$ is the design velocity at $\boldsymbol{x}^I$. For given design velocity $\boldsymbol{V}(\boldsymbol{x})$, $\dot{\Phi}^I(\boldsymbol{x})$ can be explicitly calculated even before any sensitivity analysis.

Substituting Equation (26) into the design sensitivity equation (22) and enforcing the essential boundary conditions using the mixed transformation method leads to the discrete system of equations:

$$\boldsymbol{K}^* \dot{\boldsymbol{d}} = \boldsymbol{f}^{\ell^*} - \boldsymbol{f}^{a^*} \tag{31}$$

where

$$\boldsymbol{f}^{\ell^*} = \boldsymbol{\Lambda}^{*-\mathrm{T}} \boldsymbol{f}^{\ell} \tag{32}$$

$$\boldsymbol{f}^{a^*} = \boldsymbol{\Lambda}^{*-\mathrm{T}} \boldsymbol{f}^{a} \tag{33}$$

$$\boldsymbol{f}_{\mathrm{I}}^{\ell} = \int_\Omega \Phi^{\mathrm{I}}(\nabla \boldsymbol{b} \boldsymbol{V} + \boldsymbol{b}\, \mathrm{div} \boldsymbol{V}) \mathrm{d}\Omega \tag{34}$$

$$\boldsymbol{f}_{\mathrm{I}}^{a} = \int_\Omega [\boldsymbol{B}_{\mathrm{I}}^{\mathrm{V}^{\mathrm{T}}} \boldsymbol{\sigma} + \boldsymbol{B}_{\mathrm{I}}^{\mathrm{T}} \boldsymbol{C}\, \boldsymbol{\varepsilon}^{\mathrm{V}}(\boldsymbol{z}) + \boldsymbol{B}_{\mathrm{I}}^{\mathrm{T}} \boldsymbol{\sigma}\, \mathrm{div} \boldsymbol{V}] \mathrm{d}\Omega \tag{35}$$

$$\boldsymbol{B}_I^V = -\begin{bmatrix} \Phi_{,k}^I V_{k,1} & \Phi_{,k}^I V_{k,2} & 0 \\ 0 & \Phi_{,k}^I V_{k,1} & \Phi_{,k}^I V_{k,2} \end{bmatrix}^T \tag{36}$$

The solution of Equation (31) leads to the determination of the variations $\dot{\boldsymbol{z}}$ by $\dot{\boldsymbol{z}}^R = \sum_{I=1}^{NP} (\Phi^I \dot{\boldsymbol{d}}^I + \dot{\Phi}^I \boldsymbol{d}^I)$. The sensitivity of the general performance measure (a cost or constraint function), that is,

$$\psi = \iint_\Omega g(z_i, z_{i,j})\, d\Omega \tag{37}$$

can be obtained using the direct differentiation method, as

$$\psi' = \iint_{\Omega} (g_{,z_i} \dot{z}_i + g_{,z_{i,j}} \dot{z}_{i,j})\, d\Omega + \iint_{\Omega} (g div\mathbf{V} - g_{,z_{i,j}} z_{i,k} V_{k,j})\, d\Omega \quad (38)$$

With the performance measures (cost and constraint functions) and their sensitivity information calculated by the meshfree DSA as described above, the meshfree-based shape optimization can be achieved by connecting the meshfree DSA calculation to a gradient-based optimization algorithm. In this study, the method of feasible directions (see Fox, R. L.[16]) is employed in the optimization procedure.

NUMERICAL EXAMPLES

Three automotive examples are demonstrated in the following. Design velocity vectors that represent the movement of particles in the direction of a given design parameter are computed by perturbing the design parameter. No particle re-adaptation is performed during the meshfree design optimization procedure. For comparisons, the corresponding optimization analyses in Unigraphics are also performed, where Nastran is employed for the structural analysis, HyperOpt is used as the optimization tool, and the remeshing is performed at every iteration during the shape optimization process to avoid the mesh distortion. HyperOpt utilizes the response surface optimization approach rather than a gradient-based method. To verify the reliability of the final designs, the optimum shapes resulted from the meshfree-based optimization analysis are re-meshed, and analyzed using Nastran to ensure that the stress results meet the corresponding design constraints.

Shape Design Optimization Of A Transmission Shift-Linkage Pivot Bracket

A transmission shift-linkage pivot bracket is used to change the direction of a cable running from the transmission shift linkage to the transmission in a mechanical system. In this testing, the geometry of the bracket is modeled using UG V18, and is represented by parametric coordinates as shown in Figure 2. Seven design parameters, *p0*, *p1*, *p2*, *p15*, *p26*, *p25* and *p42*, are chosen to control the shape of the bracket. A vertical load, –750N, and a horizontal load, 1500N, are applied around the upper hole. Another vertical load, 50N, is applied around the lower hole. Single-point constraints are imposed around the other two circular holes. The bracket is made of steel with E=207.4 GPa, ν=0.3, and density = 7.84E-3 kg/cm^3. The domain of the bracket is discretized by 547 RKPM particles, as shown in Figure 3. The plane stress formulation is used with a thickness of 0.3 cm.

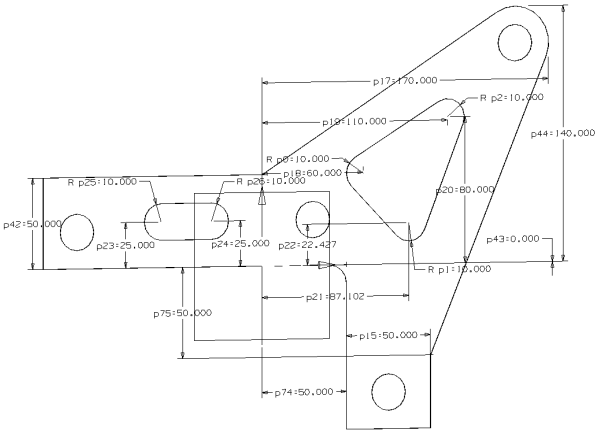

Figure 2. Design Parameterization of a Transmission Bracket

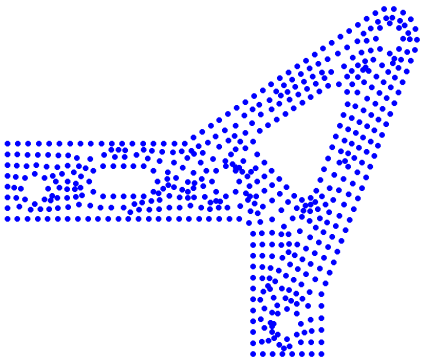

Figure 3. The Meshfree Model of The Transmission Bracket

The design optimization problem is formulated in such a way that the total mass of the structure is minimized with respect to its shape design parameters, with design constraints defined as the Von Mises stress, that is

$$\begin{aligned} &\text{minimize} && mass \\ &\text{subject to} && Von\ Mises\ Stress\ \sigma \le 200MPa \\ &\text{Design Parameters} && 45mm \le p42, p15 \le 55mm \\ & && 8mm \le p25, p26 \le 12mm \\ & && 8mm \le p0, p1, p2 \le 20mm \end{aligned} \quad (39)$$

Figure 4 shows the optimum shape resulting from the optimization analysis with RKPM and the corresponding Von Mises stress distribution.

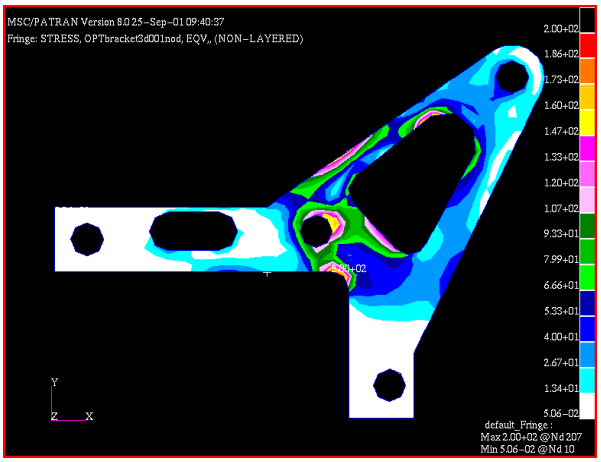

Figure 4. The Optimum Design And Its Stress Fringe of The Transmission Bracket

Figure 5 provides the optimization histories of the mass and the maximum Von Mises stress constraint from both the RKPM and UG V18 analyses. Through optimization, the structural mass in both analyses is reduced from 0.49 kg to about 0.38 kg. High oscillations in mass and stress are observed in the optimization process in UG V18, and 15 design steps are consumed to achieve the optimized design. On the other hand, 11 design steps are used in the optimization with RKPM, and a smooth convergence is demonstrated. The structural mass in RKPM steadily approaches to the minimum point without severe variations in stresses. This can be explained by the accurate computation of stress field in the analysis with RKPM, which leads to more accurate computation in the gradients of constraint/cost functions using the continuum method of shape design sensitivity analysis, and therefore results in a fast convergence of the gradient-based optimization algorithm.

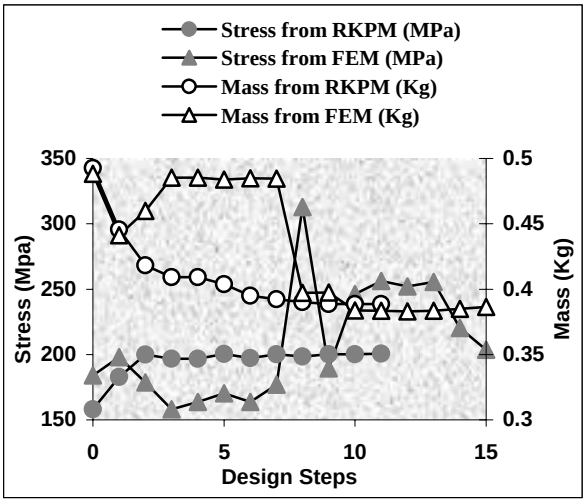

Figure 5. Histories of Design Optimization of The Transmission Bracket

Shape Design Optimization of a Torque Arm

This second example was originally presented by Bennett and Botkin[1]. The geometry of the torque arm is shown in Figure 6 and the parametric sketch of the model is in Figure 7. Four design parameters, *p6*, *p20*, *p21* and *p22*, are chosen to control the shape of the torque arm. A vertical load, 5066N, and a horizontal load, -2789N, are applied around the right-end hole. Single-point constraints are imposed around the left-end hole. The torque arm is made of steel with E=207.4 GPa, ν=0.3, and density = 7.81E-3 kg/cm^3. The domain of the torque arm is discretized by 525 RKPM particles, as shown in Figure 8. The model thickness is 0.3cm. The design optimization problem is formulated in Equation (40).

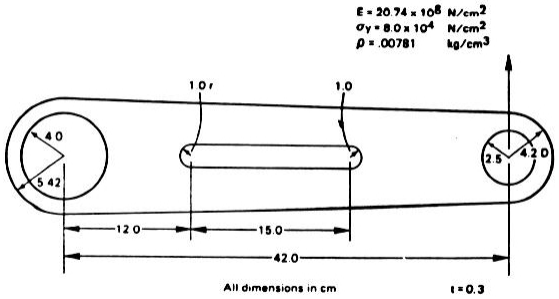

Figure 6. The Geometry of The Torque Arm

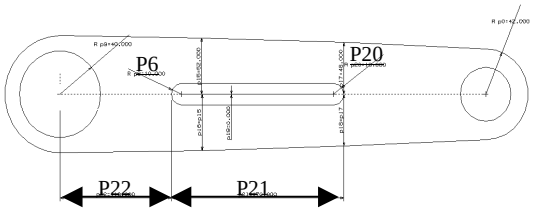

Figure 7. Design Parameterization of The Torque Arm

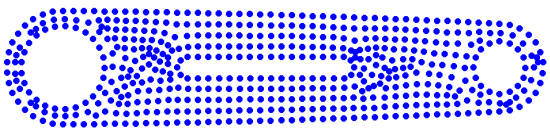

Figure 8. The Meshfree Model of The Torque Arm

$$\begin{aligned} &\text{minimize} && mass \\ &\text{subject to} && Von\ Mises\ Stress\ \sigma \le 800MPa \\ &\text{Design Parameters} && 10mm \le p6 \le 50mm \\ & && 10mm \le p20 \le 40mm \\ & && 170mm \le p21 \le 280mm \\ & && 50mm \le p22 \le 110mm \end{aligned} \quad (40)$$

Figure 9 shows the optimum shape resulting from the optimization analysis with RKPM and the corresponding Von Mises stress distribution. Figure 10 provides the optimization histories of the mass and the maximum Von Mises stress constraint resulting from both the RKPM-based design optimization procedure and the UG V18 optimization analysis. Through optimization, the structural mass is reduced from 0.91 kg to about 0.76 kg in the meshfree analysis and 0.80kg in the UG analysis. Same as the previous example, high oscillations in mass and stress are observed in UG V18 optimization process. A total of 11 design steps are consumed to achieve the optimized design in the UG V18, where only 4 design steps are used in the RKPM-based optimization. Very smooth convergences of the objective function and constraint function are observed in the RKPM-based optimization.

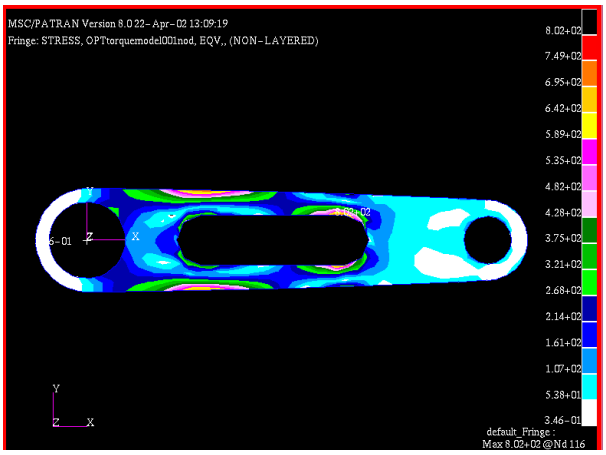

Figure 9. The Optimum Design And Its Stress Fringe of The Torque Arm

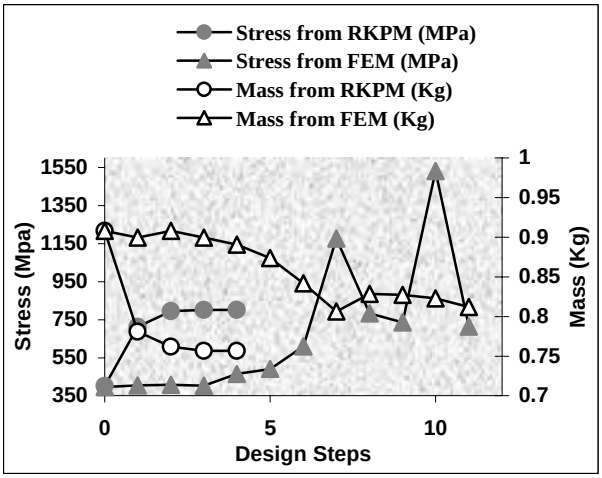

Figure 10. Histories of Design Optimization of The Torque Arm

Shape Design Optimization Of a Triangular Bracket

This example is also taken from Bennett and Botkin[1]. The geometry of the triangular bracket is shown in Figure 11. A horizontal load, 15000N, is applied around the upper hole. Single-point constraints are imposed around the lower two circular holes. The bracket is made of steel with E=207.4 GPa, ν=0.3, and density = 7.81E-10 kg/m^3. The thickness of the bracket is 0.3cm. Three design parameters, *p14*, *p34* and *p35*, as shown in Figure 12 within the circles, are chosen to control the shape of the bracket, where *p34* is equal to *p35* in the design process. The design optimization problem is formulated in Equation (41) as

$$\begin{aligned} &\text{minimize} && mass \\ &\text{subject to} && VonMises\ stress\ \sigma \le 800MPa \\ &\text{Design Parameters} && 55mm \le p14 \le 125mm \\ & && 5mm \le p34, p35 \le 20mm \end{aligned} \quad (41)$$

The domain of the bracket is discretized by 504 RKPM particles, as shown in Figure 13.

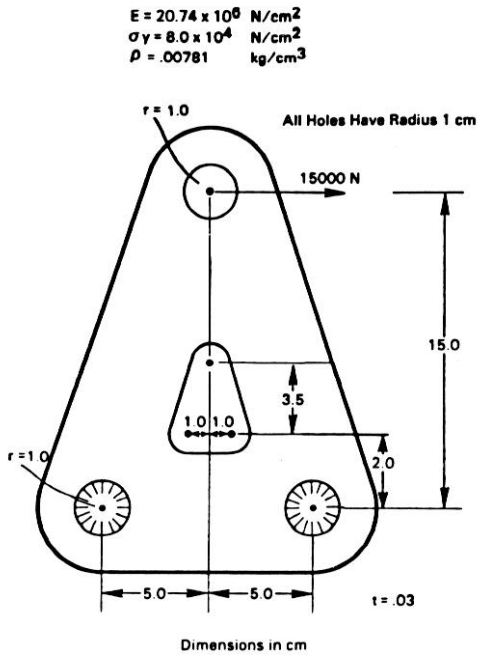

Figure 11. The Problem Description of The Triangualr Bracket

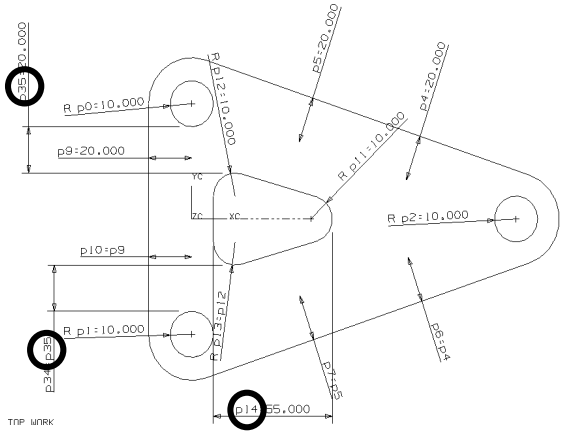

Figure 12. Design Parameterization of The Triangular Bracket

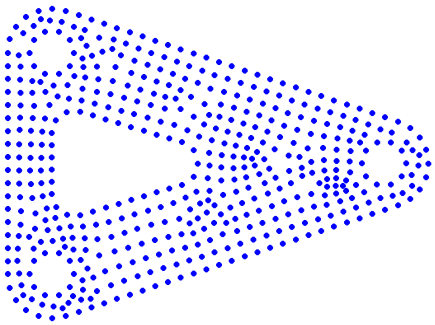

Figure 13. The Meshfree Model of The Triangular Bracket

Figure 14 shows the optimum shape resulting from the optimization analysis with RKPM and the corresponding Von Mises stress distribution. Figure 15 gives the optimization histories of the mass and the maximum Von Mises stress constraint from both RKPM and UG V18. Through optimization, the structural mass is reduced from 0.33 kg to about 0.26 kg in both the meshfree analysis and the UG analysis. Again, high oscillations in mass and stress are observed in the optimization process in UG V18, and 9 design steps are consumed to achieve the optimized design. In the optimization with RKPM, only 5 design steps are used. The structural mass in RKPM steadily approaches to the minimum point without severe variations in stresses.

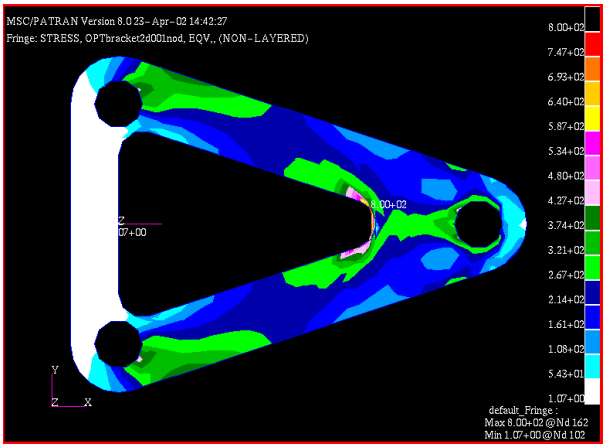

Figure 14. The Optimum Design And Its Stress Fringe of The Triangular Bracket

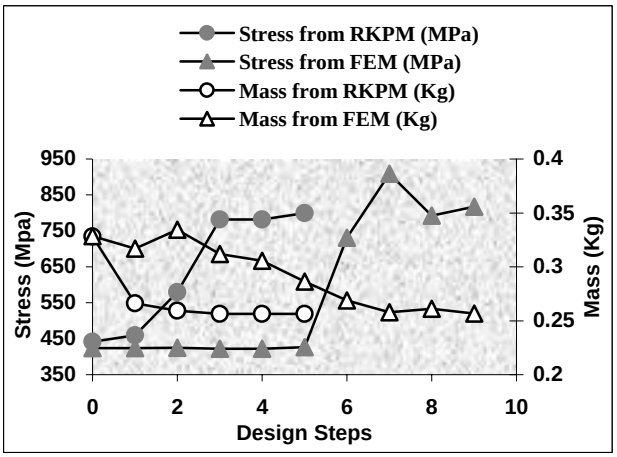

Figure 15. Histories of Design Optimization of The Triangular Bracket

CONCLUSIONS

Shape design optimization of three automotive parts, the transmission shift-linkage pivot bracket, the torque arm, and the triangular bracket, was carried out in this research using a numerical method of meshfree design sensitivity analysis and optimization. One unique feature of this method is that the approximation of unknown variables is constructed based on a set of particles scattered in the domain of interest with no requirement on the connectivity among particles. This relaxation in mesh requirements is advantageous to the analysis of problems involving large shape changes, where the mesh distortion has been problematic in the finite element solutions. The three example problems have shown that the meshfree optimization analyses could tolerate large shape changes required in the optimization process. With no need of particle re-adaptation, the meshfree-based optimization analysis still gave accurate computation of stress field and led to more accurate computation in the gradients of constraint/cost functions using the continuum method of shape design sensitivity analysis. This eventually facilitated a smooth convergence of the gradient-based design optimization algorithm, and provided optimum designs that meet the design constraints in less design iterations compared to the optimization analysis in UG V18.

ACKNOWLEDGEMENTS

Great appreciation is given to Artemis Kloess of General Motors R&D and Planning for her assistance in part of above testing.

REFERENCES

1. Bennett, J. A., and Botkin, M. E., *The optimum shape*, Plenum Press, New York, N.Y., 1986.
2. Yao, T. M., and Choi, K. K., "3–D shape optimal design and automatic finite element regridding," *Int. J. Num. Methods Eng.*, **28**, 369–384, 1989.
3. Lancaster, P., and Salkauskas, K., "Surface generated by moving least squares methods," *Math. Comp.*, **37**, 141–158, 1981.
4. Randles, P. W., and Libersky, L. D., "Smoothed particle hydrodynamics: some recent improvements and applications," *Computational Methods in Applied Mechanical Engineering*, **139**, 375–408, 1996.
5. Nayroles, B., Touzot, G., and Villon, P., "Generalizing the finite element method: diffuse approximation and diffuse elements," *Comp. Mech.*, **10**, 307–318, 1992.
6. Belytschko, T., Lu, Y. Y., and Gu, L., "Element free Galerkin method," *Int. J. Num. Methods Eng.*, **37**, 229–256, 1994.
7. Liu, W. K., Jun, S., and Zhang, Y. F., "Reproducing kernel particle methods," *Int. J. Num. Methods in Fluids*, **20**, 1081–1106, 1995.
8. Chen, J. S., Pan, C., Wu, C. T., and Liu, W. K., "Reproducing kernel particle methods for large deformation analysis of nonlinear structures," *Comput. Methods Appl. Mech. Eng.*, **139**, 195–227, 1996.
9. Melenk, J. M., and Babuska, I., "The partition of unity finite element method: basic theory and applications," *Computational Methods in Applied Mechanical Engineering*, **139**, 289–314, 1996.
10. Duarte, C. A. M., and Oden, J. T., "A H–P adaptive method using clouds," *Comput. Methods Appl. Mech. Eng.*, **139**, 237–262, 1996.
11. Grindeanu, I., Chang, K. H., Choi, K. K., and Chen, J. S., "Design sensitivity analysis of hyperelastic structures using a meshless method," *AIAA J.*, **36**, 618–627, 1998.
12. Kim, N. H., Choi, K. K., Chen, J. S., and Park, Y. H., "Meshless shape design sensitivity analysis and optimization for contact problem with friction," *Comp. Mech.*, **25**, 157–168, 2000.
13. Kim, N. H., Choi, K. K., and Chen, J. S., "Shape design sensitivity analysis and optimization of elasto-plasticity with frictional contact," *AIAA J.*, **38**, 1742–1753, 2000.
14. Kim, N. H., Park, Y. H., and Choi, K. K., "Optimization of a hyper-elastic structure with multibody contact using continuum–based shape design sensitivity analysis," *Struct. Multidisc. Optim.*, **21**, 196–208, 2001.
15. Chen, J. S., and Wang, H. P., "New boundary condition treatments in meshfree computation of contact problems," *Comput. Methods Appl. Mech. Eng.*, **187**, 441–468, 2000.
16. Fox, Richard L., *Optimization Methods For Engineering Design*, Addison-Wesley Publishing Company, Reading, Massachusetts, 1971.